Journal of Clinical and Translational Research
10.18053/Jctres/08.202206.013

ORIGINAL ARTICLE

Coronal T2-weighted imaging improves the measurement accuracy of the subarachnoid space in infants: a descriptive study

Lei Zhang[1,2†], Heng Liu[3†], Zhuanqin Ren[4], Xiaohu Wang[4], Xiaoli Meng[4], Xiaocheng Wei[1], Jian Yang[1,5*]

1. Department of Radiology, the First Affiliated Hospital of Xi'an Jiaotong University, Xi'an 710061, Shaanxi, P.R. China.
2. Department of Radiology, Baoji Hi-Tech Hospital, Baoji 721013, Shaanxi, P.R. China.
3. Medical Imaging Center of Guizhou Province, Department of Radiology, the Affiliated Hospital of Zunyi Medical University, Zunyi 563003, Guizhou, P.R. China.
4. Department of Radiology, Baoji Center Hospital, Baoji 721008, Shaanxi, P.R. China.
5. Department of Biomedical Engineering, School of Life Science and Technology, Xi'an Jiaotong University, Xi'an 710054, Shaanxi, P.R. China.

†These authors contributed equally to this work.

*Corresponding author
Jian Yang
Department of Radiology, The First Affiliated Hospital of Xi'an Jiaotong University
No. 277 West Yanta Road, Xi'an 710061, Shaanxi, P.R. China.
Tel. +86 189 9123 2396
Fax. 8629-85225009
Email: yj1118@mail.xjtu.edu.cn

Article information:
Received: August 3, 2022
Revised: October 6, 2022
Accepted: October 13, 2022

Journal of Clinical and Translational Research
10.18053/Jctres/08.202206.013

Abstract

Background: The subarachnoid space width (SASw) is part of crucial neuroimaging criteria for the diagnosis of subarachnoid space enlargement in infants. In addition to indicating the presence of these diseases, SASw can be used to assess their severity. Therefore, it is important to be able to measure the SASw accurately.

Aim: This study aimed to compare the accuracy of measurements made from axial and coronal T2-weighted imaging (T2WI), and to establish a consentaneous measurement scheme of SASw in infants.

Methods: A total of 63 infants (31 males and 32 females) aged 4 days to 24 months were enrolled in this study. The supratentorial subarachnoid space volume (SASv) and corrected SASv (cSASv) were used as the gold standard reference. The SASw (including interhemispheric width and bilateral frontal craniocortical width) was measured on axial and coronal T2WI. The intra- and interobserver reproducibility and agreement of the SASw were assessed by the intraclass correlation coefficient (ICC) and Bland-Altman analysis. A paired t-test was used to compare SASw measured on axial and coronal images. The accuracy of SASw measurements made from axial and coronal T2WI was evaluated by the relationships between the SASw and supratentorial SASv and between the SASw and supratentorial cSASv, and the relationships were examined by multivariate linear regression.

Results: The intra- and interobserver ICC values of the three SASw measurements were greater on coronal T2WI than on axial T2WI. Bland-Altman analysis confirmed that the SASw values measured on coronal T2WI had better intra- and interobserver agreement than axial T2WI. According to the multivariate linear regression results, model 4 (the SASw measured in coronal T2WI) was the best predictor of supratentorial cSASv ($R^2 = 0.755$).

Conclusions: The SASw measured on coronal T2WI was more repeatable and accurate than axial T2WI and was more representative of the actual cerebrospinal fluid accumulation in the supratentorial subarachnoid space.

Relevance for patients: The SASw has been found to be a simple and essential substitution for supratentorial SASv, which can be measured on both axial T2WI passing through the bodies of the bilateral ventricles and coronal T2WI at the level of the foramen of Monro. The SASw measured on coronal T2WI was more beneficial to the diagnosis and severity assessment of subarachnoid space enlargement in infants.

Keywords: subarachnoid space, accuracy, magnetic resonance imaging, infant

1. Introduction

The subarachnoid space width (SASw) includes interhemispheric width (IHW), sinocortical width, craniocortical width (CCW), cerebellopontine angle cistern, and Sylvian fissures [1-6]. The IHW and right and left frontal CCW (rfCCW and lfCCW) were the most commonly selected SASw indices in practical clinical medicine. SASw is part of crucial neuroimaging criteria for the diagnosis of subarachnoid space enlargement in infants. A variety of reasons can cause abnormal accumulation of cerebrospinal fluid within the subarachnoid spaces [5,7]. Benign external hydrocephalus, for instance, is a common disease in pediatric clinical practice, and neuroimaging classically shows enlargement of the subarachnoid space [1,8]. The supratentorial subarachnoid space volume (SASv) is the most direct index to evaluate cerebrospinal fluid accumulation. However, the direct measurement of supratentorial SASv remains a relatively complicated and time-consuming process, which is a major limitation of this technique from being widely used. SASw has been found to be a simple and essential means for supratentorial SASv [6,9]. In addition to indicating the presence of these diseases, SASw can be used to assess their severity [9]. Therefore, it is important to be able to measure the SASw accurately.

To date, three imaging modalities have been utilized to measure subarachnoid space: computed tomography [2], ultrasonography [3,4] and magnetic resonance imaging (MRI) [10]. The first use of CT to measure the SASw was in 1979 [2]. Currently, however, the pediatric clinical application of CT scans is limited because of the potential risk of malignancies posed by radiation, especially in infants [11]. Ultrasonography is one of the commonly preferred methods for brain imaging in infants [12]. However, the gradually closing acoustic window of the anterior fontanel limits the sensitivity and field

of view of ultrasonography [10]. Instead, it is well known that MRI is noninvasive, free of ionizing radiation and capable of providing high tissue contrast as well as high spatial resolution and has been deemed the more appropriate modality for use in infants [10,12]. The SASw can be measured on both axial T2-weighted imaging (T2WI) passing through the bodies of the bilateral ventricles [2,13] and coronal T2WI at the level of the foramen of Monro [4,14,15]. As there is currently no consentaneous measurement scheme, the definition of normal SASw in infants has varied in the previous literature [16,17]. Little is known about the relative accuracy and representativeness of SASw measured in axial and coronal T2WI, and there has been little discussion on the topic.

The purpose of this study was to establish a consentaneous measurement scheme of SASw in infants. In this study, the reproducibility and accuracy between the SASw measured on axial T2WI and coronal T2WI were compared. This was more representative of the actual cerebrospinal fluid accumulation in the supratentorial subarachnoid space.

2. Materials and methods

2.1 Subjects

The study was approved by the ethics committee (No. 2012-29) of the local hospital, and written informed consent was obtained from all parents or guardians of the subjects. Between October 2017 and August 2019, infants who came to the hospital with fever or convulsion were enrolled in this study according to the inclusion and exclusion criteria. A total of 185 infants underwent MRI to screen for brain disease. In all, 63 infants (31 males, 32 females) whose age ranged from 4 days to 24 months (4.9 ± 4.6 months) were enrolled in this study. The inclusion criterion was that infants under 24 months old

underwent a three-dimensional isotropic fast-spin-echo T2-weighted sequence (namely, 3D CUBE T2WI, GE Co.) and conventional MRI examination. The exclusion criteria were as follows: first, severe abnormal neurological symptoms or signs; second, insufficient image quality due to aliasing artifacts, motion artifacts or a low signal-to-noise ratio; and third, any condition that could cause an altered unilateral subarachnoid space according to conventional MRI examination findings, such as hypoxic-ischemic encephalopathy, white matter damage, intracranial hemorrhage, cerebral infection, trauma or malformation. A flow chart of data selection in the current research is shown in *Figure 1*.

2.2 MRI parameters

All MRI images were obtained using a 3.0-T system (Discovery MR750, GE Healthcare, Waukesha, USA) equipped with a 24-channel head coil. The infants were well sedated with oral chloral hydrate (25 mg/kg), their hearing was protected by earplugs and earmuffs before imaging, and they were continuously monitored by a pediatric nurse during the scan. 3D CUBE T2WI was performed in the sagittal plane with the following parameters: repetition time (TR) = 2000 ms, echo time (TE) = 87.3 ms, echo train length = 120, slice thickness/gap = 0.4 mm/0 mm, field of view (FOV) = 192 × 192 mm^2, matrix = 512 × 512, flip angle = 90°, number of averages = 1, number of slices to cover the entire brain = 296, and total acquisition time = 139 s. The parameters of axial T1 fluid-attenuated inversion recovery (FLAIR) were as follows: TR = 2250 ms, TE = 24 ms, inversion time (TI) = 760 ms, FOV = 192 × 192 mm^2, matrix = 256 × 256, and slice thickness/gap = 4 mm/0.4 mm. The parameters of axial T2 FLAIR were as follows: TR = 8500 ms, TE = 140 ms, TI = 1800 ms, FOV = 192 × 192 mm^2, matrix = 256 × 256, and slice thickness/gap = 4 mm/0.4 mm.

2.3 Image processing

3D CUBE T2WI was used for two purposes. First, it was used for measurement of the supratentorial SASv, which was used as the gold standard reference. Second, it was used for the reconstruction of both reformatted axial and coronal slices (reformatted slice thickness = 0.5 mm). The reference planes for axial reconstructions passed through the anterior and posterior commissures, and the coronal plane was perpendicular to the axial plane. After the reference planes were established, planes were selected for measurement of SASw. Measurement of the supratentorial SASv was performed by a fellowship-trained, board-certified neuroradiologist with Mango software (Lancaster, Martinez; http://ric.uthscsa.edu/mango/) [18,19] and MRIcro software (1.40 build 1, Neuropsychology Lab, Columbia, SC) [9,20]. The measurement process is shown in *Figure 2*. The supratentorial SASv was divided by the sum of the maximum transverse cranial diameter (TCD) and longitudinal cranial diameter (LCD), which were measured on axial images to give the corrected SASv (cSASv) to avoid the influence of individual cranial size and shape [17,21].

$$\text{cSASv} = \frac{\text{SASv}}{\text{TCD} + \text{LCD}} \quad (1)$$

Two image orientations, one axial T2WI passing through the bodies of the bilateral ventricles and one coronal T2WI at the level of the foramen of Monro, were selected for measurement of the SASw. In our study, the IHW, rfCCW and lfCCW were measured on the aforementioned axial and coronal T2WI. The IHW was defined as the maximum horizontal distance between gyri in the anterior interhemispheric fissure, and the CCW was defined as the shortest vertical distance from the inner surface of the skull to the crest of a frontal gyrus (*Figure 3*). All measurements of SASw were

performed on both axial and coronal T2WI on an Advantage Workstation (4.6, GE Healthcare, Waukesha, USA) by two other fellowship-trained, board-certified neuroradiologists blinded to the subjects' information, and one of the observers measured the SASw again after two months.

2.4 Statistical analysis

The data were analyzed by SPSS version 19.0 for Windows (SPSS, Inc., Chicago, IL, USA), and $P < 0.05$ was set as statistically significant. Continuous variables were analyzed by the one-sample Kolmogorov-Smirnov test for normality, and all parameters revealed an approximately normal distribution. The intra- and interobserver reliability and reproducibility of the SASw were assessed using the intraclass correlation coefficient (ICC). The ICC values ranged between 0 and 1, with values closer to 1 indicating higher reliability. The level of agreement within and between observers was determined by the Bland-Altman method. The results of the supratentorial SASv, cSASv and SASw are expressed as the mean ± standard deviation ($\overline{x}$ ± SD). A paired t-test was used to compare SASw measurements from axial and coronal T2WI. The relationships between the SASw and supratentorial SASv and between the SASw and cSASv were observed by univariate linear regression and multivariate linear stepwise regression. Akaike's information criterion (AIC) was chosen as the criterion to select the model; the lower the AIC value, the better the corresponding model. Finally, the optimal multivariate linear regression model and equations were established.

3. Results

3.1 Agreement analysis

The intra- and interobserver ICCs of the SASw measured on axial and coronal T2WI are listed in *Table 1*. In general, for the IHW and bilateral frontal CCW measured on axial and coronal images, all of the ICCs were greater than 0.75, and the ICCs of the three SASw variables were greater on coronal images than on axial images. The above results suggested that the SASw measurements on the coronal images had better intra- and interobserver measurement reliability and reproducibility than the corresponding measurements on the axial images.

The Bland-Altman plot and the intra- and interobserver limits of agreement (LOA, $\pm$ 1.96 $\times$ SD) of the IHW, rfCCW and lfCCW measured on the axial and coronal images were roughly the same. A representative Bland-Altman plot and the intra- and interobserver LOA of the IHW measured on the axial and coronal images are shown in *Figure 4*. Most of the scattered points were located within the LOA, and notably, the average (mean) difference was approximately 0 for the intra- and interobserver measurements of coronal images, indicating superior intra- and interobserver agreement for SASw measured on coronal images in this study.

3.2 SASv and SASw data

The supratentorial SASv ranged between 12.53 mm^3 and 281.40 mm^3 (87.97 ± 60.63 mm^3), and the cSASv ranged between 0.06 and 1.0 (0.35 ± 0.21). A summary of the IHW and bilateral frontal CCW measured on the axial and coronal T2WI by the two observers is shown in *Table 1*. The IHW and bilateral frontal CCW measured on coronal T2WI were greater than those measured on axial T2WI ($P < 0.001$, *Table 1*).

3.3 Regression analysis

First, the SASw values measured on the axial and coronal T2WI were taken as independent variables, and the supratentorial SASv and cSASv values were taken as the dependent variables to construct four univariate linear regression models (*Table 2*), as follows: model 1 – SASv (SASw measured on axial T2WI); model 2 – SASv (SASw measured on coronal T2WI); model 3 – cSASv (SASw measured on axial T2WI); and model 4 – cSASv (SASw measured on coronal T2WI). Second, the univariate linear regression model was used to screen out variables with statistical significance in the multivariate linear stepwise regression model (*Table 3*). According to the results of multivariate linear stepwise regression analysis, model 4, i.e., the SASw measured on coronal T2WI, was the most effective in predicting the cSASv ($R^2 = 0.808$). Third, however, heteroscedasticity was found when the models were evaluated; therefore, the weighted least squares method was used for estimation (*Table 4*). The above results were all subjected to a residual normality test (Shapiro-Wilk normality test), heteroscedasticity test (nonconstant variance score test) and residual autocorrelation test (autocorrelation Durbin-Watson test), and the results showed no significant difference ($P > 0.05$). The multicollinearity test showed that the variance inflation factors were all less than five, indicating weak multicollinearity between variables. After correction for heteroscedasticity, model 4, i.e., SASw measured on coronal T2WI, was the most effective in predicting the corrected volume (R2 = 0.755). The regression equations were established as follows:

$$\mathrm{cSASv} = -0.076 + 0.053 \times \mathrm{IHW} + 0.032 \times \mathrm{lfCCW} \quad (2)$$

$$\mathrm{SASv} = (-0.076 + 0.053 \times \mathrm{IHW} + 0.032 \times \mathrm{lfCCW}) \times (\mathrm{TCD} + \mathrm{LCD}) \quad (3)$$

4. Discussion

SASw is a diagnostic basis for diseases of subarachnoid space enlargement, such as benign external hydrocephalus and brain atrophy [5]. As there is currently no consentaneous measurement scheme, the definition of normal SASw in infants has varied in the previous literature [5,16,17]. The SASw can be measured on both axial images passing through the bodies of the bilateral ventricles using the same scheme applied to CT [2,13] and coronal images at the level of the foramen of Monro using the same scheme applied to ultrasonography [4,14,15]. This study suggests that the SASw measured on coronal T2WI was greater than axial T2WI and was more accurate and more representative of the actual cerebrospinal fluid accumulation in the supratentorial subarachnoid space than axial T2WI.

In this study, the SASw, including the IHW and bilateral frontal CCW, demonstrated higher intra- and interobserver repeatability when measured on coronal T2WI than axial T2WI. The reason for this result may be that there are many slices available for measurement among axial T2WI at the lateral ventricle body level [17], and different observers may choose different measurement slices. The above factor leads to significant differences in the SASw results measured on axial T2WI. In contrast, fewer slices are available for SASw measurement on coronal T2WI at the level of the foramen of Monro, resulting in less difference in the SASw results measured on coronal images.

Another observation of this study is that the SASw values measured on coronal T2WI were greater than those on axial T2WI ($P < 0.05$), which is consistent with previous reports [16,17]. Anatomically speaking, the frontoparietal convexity possesses the widest subarachnoid space anywhere in the skull [10]. Therefore, SASw measured on coronal images can best describe the subarachnoid space in this area. Furthermore, this study confirmed that model 4, consisting of SASw measured on coronal T2WI,

was significantly associated with the supratentorial cSASv, which explained 75.5% of the variability in the cSASv. On axial T2WI, the measurement line of the SASw presented an acute angle relative to the sagittal tangent of the intracranial plate, which may have increased the measured value of the SASw to be greater than the actual width. On the coronal images, however, the measurement line of the SASw was approximately perpendicular to the sagittal tangent of the intracranial plate, so the measurement value of the SASw was more consistent with reality. The above results also suggest that SASw measured on coronal images at the level of the foramen of Monro could better accurately represent the degree of cerebrospinal fluid collection in the subarachnoid space and can be used to calculate the supratentorial SASv by equations 2 and 3.

There are limitations in this study. First, the supratentorial SASv was measured by a combination of automatic and manual segmentation methods, and a long period of time was required to measure the SASv in one. Therefore, in future work, we need to further explore the application of artificial intelligence in this field, which could not only shorten the time required to measure the SASv but also improve the measurement precision. Second, due to the lack of a diagnostic gold standard for diseases in which neuroimaging classically shows enlargement of the subarachnoid space in pediatric patients, long-term follow-up observation is required to observe the prognosis of those diseases and changes in SASw or SASv with age. However, this does not affect the reliability of the results in this study because this was a controlled study of the SASw measurement method.

Conclusions

The SASw measurement using coronal T2WI was a simpler, more reproducible, and more accurate

method than those measurements using axial images. The former measurement yielded values that were more representative of the actual supratentorial SASv and could be used to establish a unified normal standard for SASw. This study suggests that SASw measured on coronal T2WI should be a preferred measurement scheme in infants, as should other imaging modalities.

Acknowledgments: We would like to thank Dr. Miaomiao Wang (Department of Radiology, the First Affiliated Hospital of Xi'an Jiaotong University) for giving important advice. This study was supported by the National Natural Science Foundation of China (No. 81771810, 81971581); the Innovation Capability Support Program of Shaanxi (No. 2019TD-018); the Clinical Research Award of the First Affiliated Hospital of Xi'an Jiaotong University (No. XJTU1AF-CRF-2020-005); and the Health Research Fund Project of Shaanxi Province [No. 2018C001]. It was approved by the local Institutional Review Board (No. 2012-29) and all the informed written consents were obtained from all parents or guardians of participants.

Conflict of interest

None.

References

1. Andersson J, Wikström J, Högberg U, Wester K, Thiblin I. External Hydrocephalus as a Cause of Infant Subdural Hematoma: Epidemiological and Radiological Investigations of Infants Suspected of Being Abused. Pediatr Neurol. 2022;126:26-34.

2. Fukuyama Y, Miyao M, Ishizu T, Maruyama H. Developmental changes in normal cranial measurements by computed tomography. Dev Med Child Neurol 1979;21:425-432.

3. Lam WW, Ai VH, Wong V, Leong LL. Ultrasonographic measurement of subarachnoid space in normal infants and children. Pediatr Neurol 2001;25:380-384.

4. Libicher M, Tröger J. US measurement of the subarachnoid space in infants: normal values. Radiology 1992;184:749-751.

5. Zahl SM, Egge A, Helseth E, Wester K. Benign external hydrocephalus: a review, with emphasis on management. Neurosurg Rev 2011;34:417-432.

6. Watanabe Y, Abe S, Takagi K, Yamamoto T, Kato T. Evolution of subarachnoid space in normal fetuses using magnetic resonance imaging. Prenat Diagn 2005;25:1217-1222.

7. Halevy A, Cohen R, Viner I, Diamond G, Shuper A. Development of infants with idiopathic external hydrocephalus. J Child Neurol 2015;30:1044-1047.

8. Zahl SM, Egge A, Helseth E, Wester K. Clinical, radiological and demographic details of benign external hydrocephalus: A population-based study. Pediatr Neurol 2019;96:53-57.

9. Brett M, Leff A, Rorden C, Ashburner J. Spatial normalization of brain images with focal lesions using cost function masking. NeuroImage 2001;14:486-500.

10. Orrù E, Calloni SF, Tekes A, Huisman TAGM, Soares BP. The child with macrocephaly: Differential diagnosis and neuroimaging findings. Am J Roentgenol 2018;210:848-859.

11. Pearce MS, Salotti JA, Little MP, et al. Radiation exposure from CT scans in childhood and subsequent risk of leukaemia and brain tumours: a retrospective cohort study. Lancet 2012; 380:499-505.

12. Paciorkowski AR, Greenstein RM. When is enlargement of the subarachnoid spaces not benign? A genetic perspective. Pediatr Neurol 2007;37:1-7.

13. McArdle CB, Richardson CJ, Nicholas DA, Mirfakhraee M, Hayden CK, Amparo EG. Developmental features of the neonatal brain: MR imaging. Part II. Ventricular size and extracerebral space. Radiology 1987;162:230-234.

14. Leijser LM, Srinivasan L, Rutherford MA, Counsell SJ, Allsop JM, Cowan FM. Structural linear measurements in the newborn brain accuracy of cranial ultrasound compared to MRI. Pediatr Radiol 2007;37:640-648.

15. Tucker J, Choudhary AK, Piatt J. Macrocephaly in infancy: benign enlargement of the subarachnoid spaces and subdural collections. J Neurosurg Pediatr 2016;18:16-20.

16. Wiig US, Zahl SM, Egge A, Helseth E, Wester K. Epidemiology of Benign External Hydrocephalus in Norway-A Population-Based Study. Pediatr Neurol 2017;73:36-41.

17. Hussain ZB, Hussain AB, Mitchell P. Extra-axial cerebrospinal fluid spaces in children with benign external hydrocephalus: A case-control study. Neuroradiol J 2017;30:410-417.

18. Lancaster JL, Cykowski MD, McKay DR, et al. Anatomical global spatial normalization. Neuroinformatics 2010;8:171-182.

19. Yeatman JD, Richie-Halford A, Smith JK, Keshavan A, Rokem A. A browser-based tool for visualization and analysis of diffusion MRI data. Nat Commun 2018;9:940.

20. Chen X, Chen Y, Xu Y, Gao Q, Shen Z, Zheng W. Microstructural and neurochemical changes in the rat brain after diffuse axonal injury. J Magn Reson Imaging 2019;49:1069-1077.

21. Prassopoulos P, Cavouras D. CT evaluation of normal CSF spaces in children: relationship to age, gender and cranial size. Eur J Radiol 1994;18:22-25.

Figures and tables

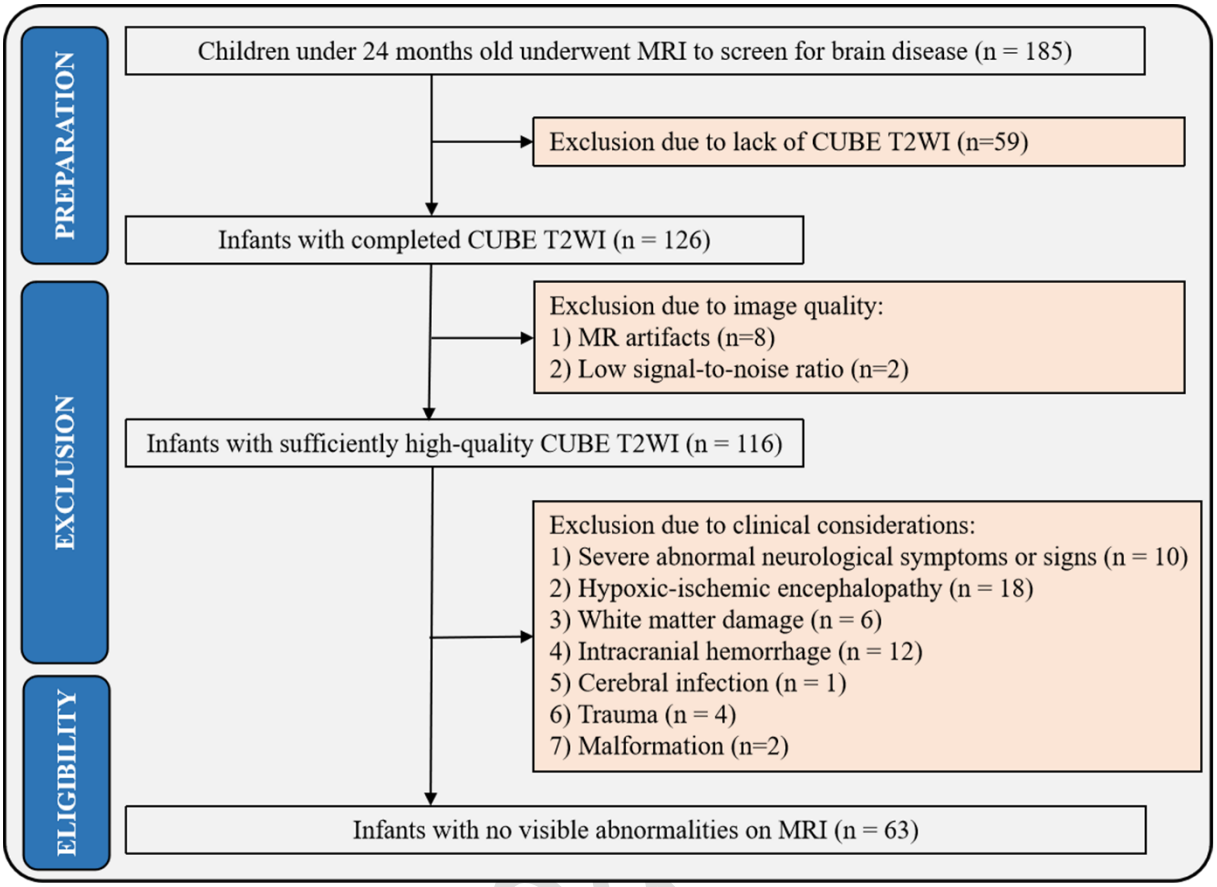

Figure 1. Flow chart for the selection of research subjects based on the inclusion and exclusion criteria.

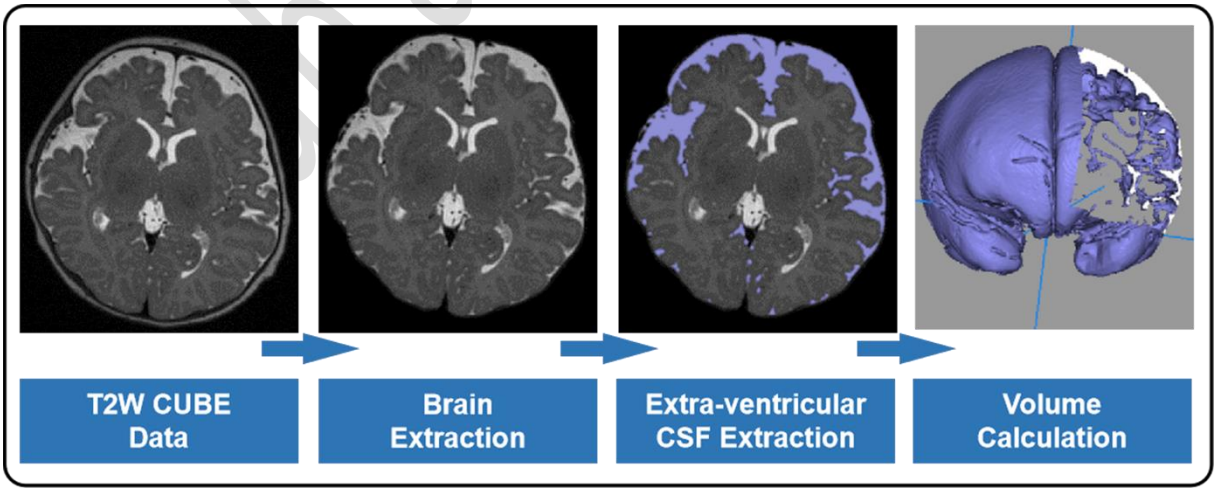

Figure 2. The process of supratentorial subarachnoid space volume measurement.

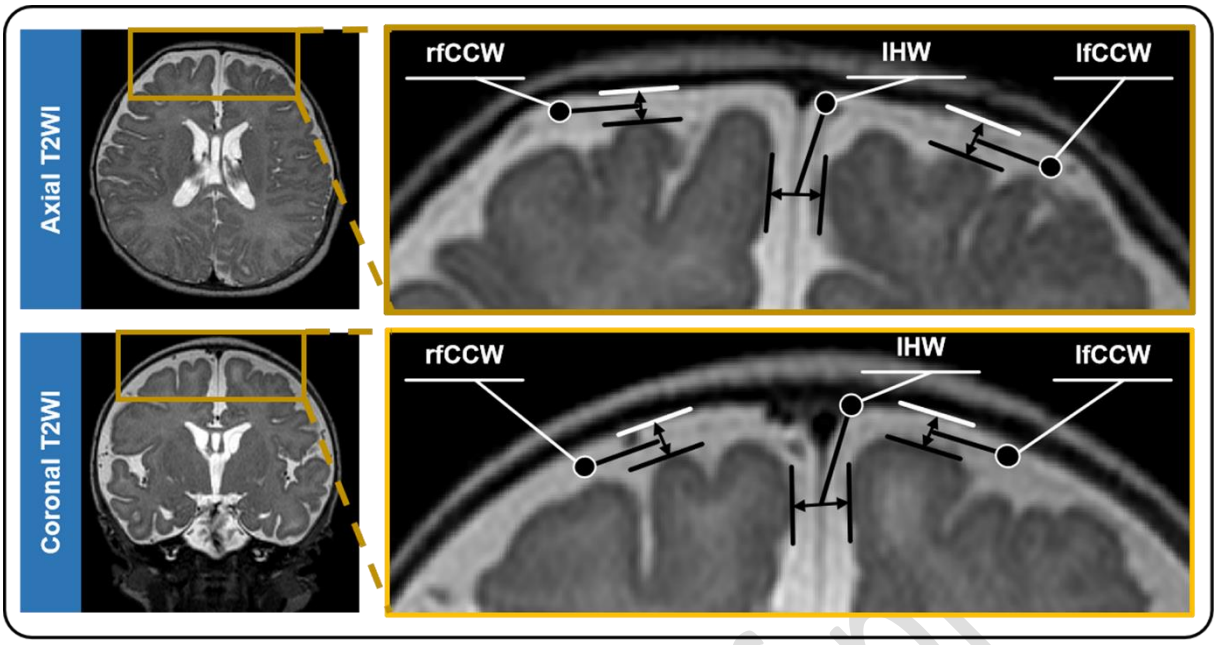

Figure 3. Schematic diagram of the procedure for subarachnoid space width (SASw) measurements. The interhemispheric width (IHW) and the right and left frontal craniocortical width (rfCCW and lfCCW, respectively) on an axial image (upper) and a coronal image (lower).

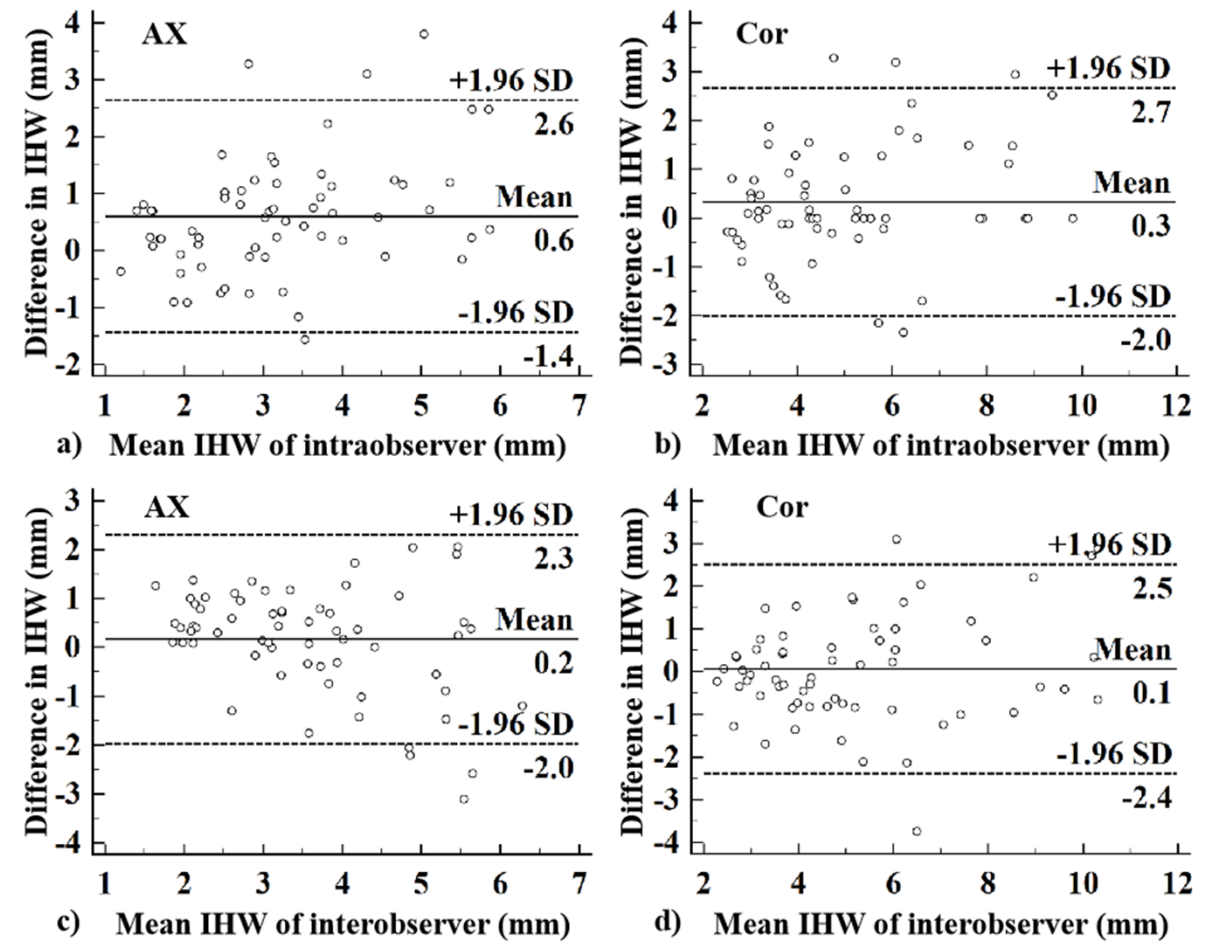

Figure 4. Bland-Altman plots showing the intraobserver (a, b) and interobserver (c, d) variability of the interhemispheric width (IHW). The difference in IHW of intra- and interobserver measurements (y-axis) was plotted against the average measurement (x-axis). The horizontal lines indicate the mean difference of the intra- and interobserver measurements (solid) and the limits of agreement (dotted).

Journal of Clinical and Translational Research
10.18053/Jctres/08.202206.XXX

Table 1. The SASw measured on axial and coronal images

				Interhemispheric width		Frontal cranio-cortical width			
						Right		Left	
				AX	Cor	AX	Cor	AX	Cor
Reliability analysis of SASw (intraclass correlation coefficients)		Intraobserver		0.824	0.905	0.841	0.871	0.794	0.899
		Interobserver		0.801	0.919	0.833	0.901	0.837	0.896
SASw (mm)	Observer 1	1st test	$\overline{x}$ ± SD	3.5 ± 1.5	5.2 ± 2.2	2.5 ± 1.0	4.5 ± 1.6	2.5 ± 0.9	4.4 ± 1.4
		2nd test	$\overline{x}$ ± SD	2.9 ± 1.2	4.8 ± 1.9	2.1 ± 1.0	3.9 ± 1.3	2.2 ± 1.0	3.9 ± 1.3
	Observer 2		$\overline{x}$ ± SD	3.7 ± 1.2	5.2 ± 2.4	3.0 ± 1.2	4.5 ± 1.6	2.9 ± 1.2	4.6 ± 1.8
Comparison of SASw between AX and Cor (Paired-samples *t*-test)			*t* value	6.615		10.924		9.342	
			P value	< 0.001		< 0.001		< 0.001	

* AX, axial images; Cor, coronal images; SASw, subarachnoid space width.

Table 2. The univariate linear regression (n=63)

Variate	Model 1 - SASv on AX			Model 2 - SASv on Cor			Model 3 - cSASv on AX			Model 4 - cSASv on Cor		
	IHW	rfCCW	lfCCW	IHW	rfCCW	lfCCW	IHW	rfCCW	lfCCW	IHW	rfCCW	lfCCW
Regression coefficient	31.094	31.845	28.976	21.195	28.734	26.345	0.112	0.112	0.104	0.074	0.102	0.094
Standard error	5.392	5.171	5.494	1.736	3.077	2.645	0.018	0.017	0.018	0.005	0.010	0.008
t	5.766	6.158	5.274	12.212	9.338	9.962	6.267	6.499	5.721	13.523	10.525	11.315
P	<0.001	<0.001	<0.001	<0.001	<0.001	<0.001	<0.001	<0.001	<0.001	<0.001	<0.001	<0.001
R^2	0.353	0.383	0.313	0.710	0.588	0.619	0.392	0.409	0.349	0.750	0.645	0.677
Corrected R^2	0.342	0.373	0.302	0.705	0.582	0.613	0.382	0.399	0.339	0.746	0.639	0.672

***** AX, axial images; Cor, coronal images; SASv, subarachnoid space volume; cSASv, corrected subarachnoid space volume; IHW, interhemispheric width; lfCCW, left frontal cranio-cortical width; rfCCW, right frontal cranio-cortical width.

Table 3. The multivariate linear stepwise regression (n=63)

Variate	Model 1 - SASv on AX			Model 2 - SASv on Cor			Model 3 - cSASv on AX			Model 4 - cSASv on Cor		
	Intercept	rfCCW	IHW	Intercept	IHW	lfCCW	Intercept	rfCCW	IHW	Intercept	IHW	lfCCW
Regression coefficient	- 46.240	21.674	19.195	- 39.783	14.644	11.255	- 0.127	0.075	0.071	- 0.102	0.049	0.043
Standard error	19.471	5.693	5.795	10.575	2.541	3.381	0.064	0.019	0.019	0.032	0.008	0.010
t	- 2.375	3.807	3.313	- 3.762	5.763	3.329	- 2.004	4.012	3.730	- 3.204	6.386	4.257
P	0.021	< 0.001	0.002	< 0.001	< 0.001	0.001	0.050	< 0.001	< 0.001	0.002	< 0.001	< 0.001
R^2		0.479			0.755			0.520			0.808	
Corrected R^2		0.461			0.747			0.504			0.801	

***** AX, axial images; Cor, coronal images; SASv, subarachnoid space volume; cSASv, corrected subarachnoid space volume; IHW, interhemispheric width; lfCCW, left frontal cranio-cortical width; rfCCW, right frontal cranio-cortical width.

Table 4. The multivariate linear regression with weighted least squares method (n=63)

Variate	Model 1 - SASv on AX			Model 2 - SASv on Cor			Model 3 - cSASv on AX			Model 4 - cSASv on Cor		
	Intercept	rfCCW	IHW	Intercept	IHW	lfCCW	Intercept	rfCCW	IHW	Intercept	IHW	lfCCW
Regression coefficient	- 52.378	16.082	25.505	- 25.055	16.212	6.064	- 0.159	0.058	0.093	- 0.076	0.053	0.032
Standard error	15.650	5.082	5.647	7.682	2.941	3.021	0.051	0.017	0.019	0.025	0.009	0.010
t	- 3.347	3.164	4.516	- 3.261	5.513	2.007	- 3.100	3.497	5.013	- 3.075	5.670	3.346
P	0.001	0.002	< 0.001	0.002	< 0.001	0.049	0.003	0.001	< 0.001	0.003	< 0.001	0.001
R^2		0.52			0.69			0.57			0.76	
Corrected R^2		0.50			0.68			0.55			0.75	

***** AX, axial images; Cor, coronal images; SASv, subarachnoid space volume; cSASv, corrected subarachnoid space volume; IHW, interhemispheric width; lfCCW, left frontal cranio-cortical width; rfCCW, right frontal cranio-cortical width.